Effect Of Accelerated Ageing Cycles On The Physical And Mechanical Properties Of A Reversible Thermoplastic Adhesive

The Journal of Adhesion

ISSN: 0021-8464 (Print) 1545-5823 (Online) Journal homepage: https://www.tandfonline.com/loi/gadh20

Effect Of Accelerated Ageing Cycles On The Physical And Mechanical Properties Of A Reversible Thermoplastic Adhesive

R. Ciardiello, G. Belingardi, B. Martorana & V. Brunella

To cite this article: R. Ciardiello, G. Belingardi, B. Martorana & V. Brunella (2018): Effect Of Accelerated Ageing Cycles On The Physical And Mechanical Properties Of A Reversible Thermoplastic Adhesive, The Journal of Adhesion, DOI: 10.1080/00218464.2018.1553714

To link to this article: https://doi.org/10.1080/00218464.2018.1553714

Published online: 03 Dec 2018.

THE JOURNAL OF ADHESION
https://doi.org/10.1080/00218464.2018.1553714

Taylor & Francis
Taylor & Francis Group

Effect Of Accelerated Ageing Cycles On The Physical And Mechanical Properties Of A Reversible Thermoplastic Adhesive

R. Ciardiello[a], G. Belingardi[a], B. Martorana[b], and V. Brunella[c]

[a]Department of Mechanical and Aerospace Engineering, Politecnico di Torino, Torino, Italy; [b]Group Materials Labs, Centro Ricerche Fiat S.C.p.A., Torino, Italy; [c]Department of Chemistry and NIS Research Centre, University of Torino, Torino, Italy

ABSTRACT

In this work, a polyolefin thermoplastic adhesive has been modified with three different weight percentages, 3%, 5% and 10% of iron oxide powder. The use of this nano-modified adhesive coupled with this technology, offers an improved resistance to applied loads, new opportunities connected with the bonding process and the possibilities to dismantle plastic components for reusing, repairing or recycling at the end of life. In this research activity, the mechanical properties of the pristine and modified adhesive have been assessed. Furthermore, the effect of three different accelerated ageing cycles, currently used by automotive industries, have been studied in relation to the mechanical behaviour and separation time. Three ageing cycles were evaluated that are: hot, humid and mixed cycles. Single Lap Joint tests prove the variations of the mechanical properties and adhesion strength during the accelerated ageing, especially for the hot cycle. Fourier Transform Infrared Spectroscopy has been used and shows that the adhesives exposed to the hottest ageing cycle presented a high value of the oxidation that leads to a partial detachment of the adhesive from the plastic substrates. Joint separations by means of an induction heating system showed that adhesive joints can be separated before and after ageing cycles.

ARTICLE HISTORY
Received 27 November 2018
Accepted 27 November 2018

KEYWORDS
Reversible adhesive joint; hot-melt adhesive; magnetite nanoparticles; ageing; accelerated ageing

1. Introduction

Recently, vehicles are designed lighter in order to reduce air pollution and fuel consumption. In the last decade, the use of composite and plastic materials increased a lot since they represent a real possibility to lighten the vehicle weight.[1] This trend led to a wider use of adhesive joints since they represent an easy and efficient way to join these materials[2,3] due to their good resistance to fatigue and corrosion, their uniform stress distribution compared to the traditional mechanical fasteners and moreover they

CONTACT R. Ciardiello raffaele.ciardiello@polito.it
Color versions of one or more of the figures in the article can be found online at www.tandfonline.com/gadh.

result in weight reduction. One of the most used plastic materials that has been widely adopted recently by automotive industries is the polypropylene and the related copolymers.[4] These thermoplastic materials are very difficult to bond and one of the most effective ways to join parts made with this material is the use of polyolefin thermoplastic adhesive.[5] The European Directive 2000/53/EC on end-of-life of vehicles (ELV Directive) sets out the requirement to limit the polluting waste and promote the reuse, recycle and recover of components, in particular the plastic ones, at the end of the life cycle. The traditional techniques for disassembling are too complex and long to be adopted in vehicle industries.[6] These techniques use iron oxide nanoparticles, Fe_3O_4, that are sensitive to the electromagnetic field, in order to heat the adhesive up to its melting point.[7,8] The particles are embedded into the adhesive matrix and, when submitted to alternate electromagnetic field excitation, heat up because of hysteresis losses, and the Neel and Brown relaxation effect.[9–14] A similar process configuration has been used by Banea et. al[15] and Severijns et al..[16] Furthermore, Banea et al.[17] described some methods that allow for an easy disassembly on command of adhesive structural joints. Although these nanomodified adhesives can represent a valid possibility to separate thermoplastic adhesive joints, the use of nanoparticles in these adhesives might lead to detrimental effects on the mechanical properties or to inadequate response to environmental factors and therefore it is necessary to study these aspects.

The literature is rich of basic and complex ageing processes related to adhesives used for bonding composite materials.[18–20] Pethrick[21] reported a review on the performances of structural adhesives may vary because of the stress induced by thermal effects and hygrothermal factors. This review described that the performance and durability of a joint prepared with metal and carbon fibre composites depend on the stability of the interface between adhesive and adherend. Viana et al[22] reported detailed review about the effect of the combination of moisture and temperature degradation of the adhesive joints and it describes that this combination may influence the bulk behaviour of adhesive. On the other hand, there are only a few works about procedures able to study the ageing effect on the thermoplastic adhesives.[23,24] The ISO 188:2011[25], illustrates an accelerated ageing and heat resistance method to evaluate the mechanical properties of thermoplastic rubber. The standard specifies that the testing temperature should be equal to the operative temperature. On the other hand, ASTM D5721[26] illustrated a test method for the ageing of polyolefin geomembranes. However, we are interested in polyolefin adhesives that are used as thermoplastic adhesives for many internal and external automotive applications.[5] The mentioned ASTM standard illustrates a hot ageing cycle where the maximum temperature is maintained below the adhesive softening point. Both Koricho et al.[23] and Ciardiello et al.[24] reported three different ageing

cycles, the same that have been used in this work as well, for thermoplastic adhesives. These cycles have been proposed by automotive industries in order to study the ageing properties of these adhesive. The main philosophy behind these cycles is to expose the adhesive joints for several days to severe thermal and humidity conditions.

In this work, the mechanical behaviour and the ageing effect for a pristine and nanomodified hot melt adhesives (HMA) were studied by using single lap joint tests. This adhesive is a polyolefin thermoplastic non-reactive adhesive. Three ageing cycles (namely A, B and C) have been used. Cycle A is an ageing cycle close to the ones proposed by ASTM D5721 and ISO 188:2011 with a thermal exposure of the SLJ specimens at a relatively high temperature, 90°C. Cycle B is an ageing cycle that simulates a humid severe environment, 40°C with 98% of relative humidity. Finally, Cycle C combines a sequence of hot, humid and cold temperature conditions maintained for shorter time. The main aim of the cycle C is to submit the adhesive joint at severe environmental condition in order to stress the joints and verify possible detachments or induced stresses that could be detrimental for the mechanical performances due to the change of environmental conditions. The separation tests of the nanomodified adhesive joints were carried out, by means of an inductor, before and at the end of the ageing cycles in order not only to prove that joint separation is possible also at the end of the ageing cycles but also to assess the residual joint separation performance after the ageing cycles. FTIR analysis was used in order to control eventual oxidation of the adhesive. Finally, SEM analysis is presented in order to verify the distribution of the nanoparticles inside the adhesive matrix.

2. Materials and methods

The adherents used for this experimental activity are made of polypropylene (PP) copolymer (Hifax CB 1160 G1, by Lyondell-Basell Industries, Houston, United States) with 10% by weight of talc. These adherends are 100 mm long and they have cross-section of 20 × 3 mm, as showed in Figure 1. PP copolymer are widely used in in automotive industry for internal and external applications, such as plastic bumper, tail gate and many aesthetic skins.

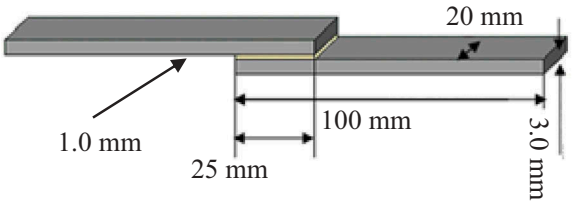

Figure 1. Single Lap Joint specimen.

The substrates were bonded with Prodas, a polyolefin-based thermoplastic HMA by Beardow Adams (Milton Keynes, United Kingdom), a copolymer of polypropylene and polyethylene. The nanomodified adhesive was prepared in our lab using a hot plate for melting the neat adhesive and adding three different weight percentages of iron oxide: 3%, 5%, and 10%. Based on manufacturer datasheet, iron oxide particles have a particle size smaller than 50 nm (Fe_3O_4 by Sigma-Aldrich, Saint Louis, United States). Table 1 reports the physical properties of the pristine HMA from the datasheet. The glass transition temperature was calculated by means of differential scanning calorimetry.[23]

Mechanical tests were carried out on the Single Lap Joint (SLJ) specimens. The geometry of the SLJ is shown in Figure 1. The overlap and adhesive layer thickness were varied to study the influence of these two parameters on the maximum strength. The typical sizes of the bonded joint are shown in Figure 1. These values were chosen based on a preliminary experimental analysis presented by Koricho et al..[23]

Following a procedure commonly adopted in the literature for the preparation of modified HMAs in the lab[5,7,8,23,24,27], pellets were melted together at 190°C, using a hot plate. At 190°C, the viscosity of this adhesive is low enough to easily mix the particles into the adhesive by mean of a glass rod. The iron oxide nanoparticles were added gradually and mixed together with the adhesive. The joint preparation was performed by using a hot-melt gun and an assembly device, shown in Figure 2, which makes it possible to control the thickness of the adhesive joint. Each substrate was cleaned with isopropyl alcohol (IPA) before the joint preparation. The SEM analysis in the next section shows that the modified adhesives present some particle clusters that are very similar to the as received particles as showed in.[27]

As shown in Figure 2, a film-thickness controller screw was used to fix the thickness of the adhesive layer at the desired value. Firstly, one adherent, the lower substrate in Figure 2, was fixed on the lower base of the assembly device. Then, the HMA at high temperature, 190°C, was uniformly spread over the lower substrate by means of the hot-melt gun. An amount of adhesive larger than necessary was used to ensure that the overlap of the lower substrate was completely covered. Then, the other adherend, the upper

Table 1. Physical properties of the hot-melt adhesive.

Melting temperature (Initial – Final)	124°C – 155°C
Viscosity at 180°C (S. 27/5 rpm) (BA QA102)	22–28 Pa*s
Glass transition temperature	−14°C
Open time	30 s
Density	0.98 g/cm^3
Initial thermal degradation temperature	210°C

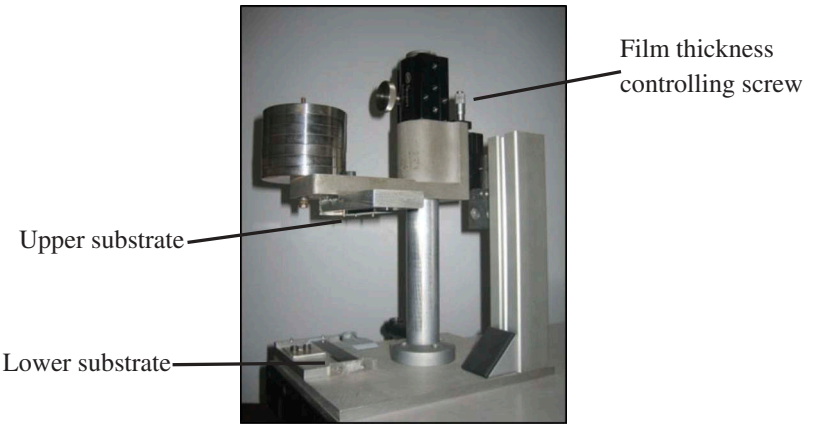

Figure 2. Instrumentation used for the adhesive joint preparation: a) hot-melt gun; b) assembly device.

substrate in Figure 2, was placed on the still melted adhesive. A mass of (3.5 kg) was placed on the support of the upper adherend. The presence of this weight ensures that the excess adhesive is squeezed out until the required adhesive thickness was reached. After the adhesive solidification, the excess adhesive was removed by means of a cutter. The assembly device permits to control the overlap length and the adhesive layer thickness that presented a variation smaller than 0.03 mm. Tabs were bonded to the substrate extremities to avoid misalignment, as specified by the standards.

The SLJ tests were conducted at a constant displacement rate of 100 mm/min, according to the FCA (Fiat Chrysler Automobile) standard on the hot-melt adhesive, using an Instron 8801 servo-hydraulic machine. This configuration was used also in.[5,7,8,23,24,27] At least five replications were carried out for each adhesive composition.

2.0.1. *Ageing cycles*

The mechanical properties of pristine and nanomodified HMA were also studied during and after the ageing cycles. The used ageing cycles were defined in an FCA standard. The ageing cycles are:

Cycle A: Exposure at 90°C without the control of the Relative Humidity (RH) for 500 h.

Cycle B: Exposure at 40°C with RH set at 98% for 500 h.

Cycle C: Exposure at 80 °C without RH for 24 hours,

Exposure at 40°C with RH set at 98% for 24 hours,

Exposure at −40°C for 24 hours.

Ageing cycles were carried out by using Votsch VT4020 and Votsch Heraeus HC0020 chambers (maximum temperature fluctuation ±0.3°C). The mechanical properties of the adhesives were assessed at progressive stages during the ageing cycles. SLJ tests for cycles A and B were performed after one week, two

weeks and at the end of the cycles (500 h for the cycles A and B) in order to verify the mechanical properties of SLJ during the ageing cycles. SLJ tests for the cycle C were carried out at the end of the cycle (72 h).

2.0.2. *Separation tests*

Beside the SLJ tensile tests, also separation tests were performed: they are finalised to measure the separation time that is the time elapsed from the application of the external magnetic field until the consequent joint separation. The inductor used for this analysis is Heasyheat by Ambrell, with a maximum power of 10 kW and a frequency range from 10 to 400 kHz. Based on the results of preliminary tests, for all these separation tests, the frequency of the electromagnetic field was set 314 kHz and the applied power was set 6 kW. For each test, a mass of 0.5 kg was applied to the SLJ lower extremity in order to submit the adhesive joint to a constant load and initiate the bonded joint separation (by part sliding) when the joint adhesive reaches its melting temperature. The configuration for the separation test is shown in Figure 3. Five replications were carried out for both the non-aged and aged specimens.

2.0.3. *Scanning electron microscope*

Scanning electron microscopy (SEM) analyses were carried out by using a ZEISS EVO 50 XVP microscope with LaB6 source, equipped with detectors for secondary electrons collection and energy dispersive X-ray probe (EDS) for elemental analysis. SEM micrographs were obtained after sputtering samples with ca. 15 nm of a gold layer to avoid any charging effect (Bal-tec SCD050 sputter coater). For these analyses, the high tension at 20 kV and the secondary electron emission signal were used.

2.0.4. *Fourier transform infrared analysis*

Fourier Transform Infrared (FTIR) spectra were recorded in the spectral range of 4000–650 cm^{-1} using a Perkin Elmer Spectrum 100 instrument in the attenuated total reflectance (ATR) mode with a diamond crystal, using 32 scans per spectrum and a resolution of 4 cm^{-1}.

3. Results and discussion

3.1. *Nomenclature*

In the following sections, HMA is referring to the pristine hot-melt adhesive, HMA_3%, HMA_5% and HMA_10%. are referring to the adhesive modified with the 3% wt., 5% wt. and 10% wt., respectively.

Figure 3. Configuration for the adhesive joint separation.

3.2. *Single lap joint tests*

Figure 4 shows the typical load-displacement curves of SLJ tests for the four different adhesive formulations. The curves in Figure 4 are relative to the SLJ with an overlap of 25 mm and an adhesive layer thickness of 1 mm and are representative for the replications that have been carried out. The pristine HMA is the solid curve that is the lowest curve in the diagram. As illustrated, the increase of the particles content brings to an increase of the maximum loads and to a more

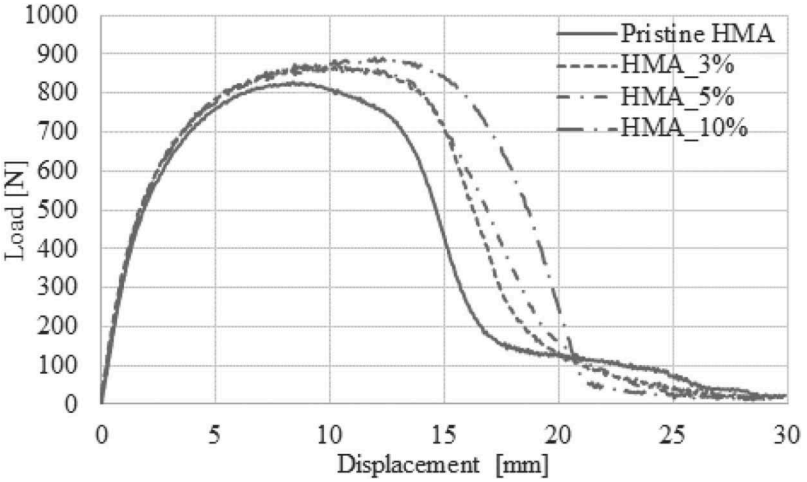

Figure 4. Representative curves of SLJ tests of the different adhesive compositions.

ductile behaviour of the modified HMAs, as can be noted by the larger values on the right part of the curves. The nanomodified adhesives also have larger elongations compared to pristine HMA. Mechanical properties of HMA_3% and HMA_5% are very close. As can be noted the initial parts of the curves are superimposed for all the adhesive compositions. The increase of the maximum loads for the nanomodified adhesives could be due to the micro agglomerates that are shown in the following SEM section. This agglomerates lead to a toughening of the bondline that resulted in an increase of the maximum shear strength as explained by.[28,29] Table 2 reports the average maximum loads, the shear strengths, the stiffness and the elongations of the joints for all the adhesive compositions. The average maximum load and strength shows that the adhesive joints prepared with the modified HMA increased. The stiffness, calculated on the adhesive joints prepared with the four adhesive compositions, do not change, as expected since the linear trends of the curves relative to the modified adhesives are superimposed to the pristine one. Finally, the values of the elongations were calculated on the maximum displacement as done in. [7] The displacement values were measured when the load decreased down to 200N since this is the load at which all the curves drop, as can be seen in Figure 4. This value has been preferred

Table 2. Mechanical properties of the adhesive joints with the values of the standard deviation (in brackets).

	Pristine HMA	HMA_3%	HMA_5%	HMA_10%
Average maximum load [N]	835.55 (22.52)	878.15 (20.27)	881.45 (30.84)	895.14 (16.66)
Maximum shear strength [MPa]	1.67 (0.04)	1.75 (0.04)	1.76 (0.06)	1.79 (0.03)
Stiffness [MPa]	14.3 (0.2)	14.3 (0.2)	14.5 (0.4)	14.3 (0.2)
Elongations [%]	62.5 (2.0)	73.8 (3.8)	80.4% (6.2)	81.0 (0.8)

to the displacement corresponding to the load of zero because the adhesive had very high elongation, in some cases, and so the results can be affected by this behaviour. The elongations increase for the adhesive joint relative to the modified adhesives.

3.3. *Ageing tests*

Figure 5 shows representative curves of the SLJ tests during and after the accelerated cycles A, B and C, related to the pristine adhesive. The diagrams show the progressive change in the load-displacement curves with ageing time. Figure 5a, that is related to the cycle A, evidence that this cycle is the most aggressive for the pristine HMA, since the maximum load decreases of 47% and the end of the ageing. The progressive drops of the average maximum load during the 3 weeks are respectively 25%, 16% and 6%. This means that there is a huge decrease of the average maximum load at the beginning of the cycle A and then there is a sort of stabilization since the average maximum load tends to converge to a lower value. Furthermore, the curves of SLJ tests carried out during and at the end of the ageing cycle A resulted in a progressive reduction, not only of the maximum load but of the elongations as well.

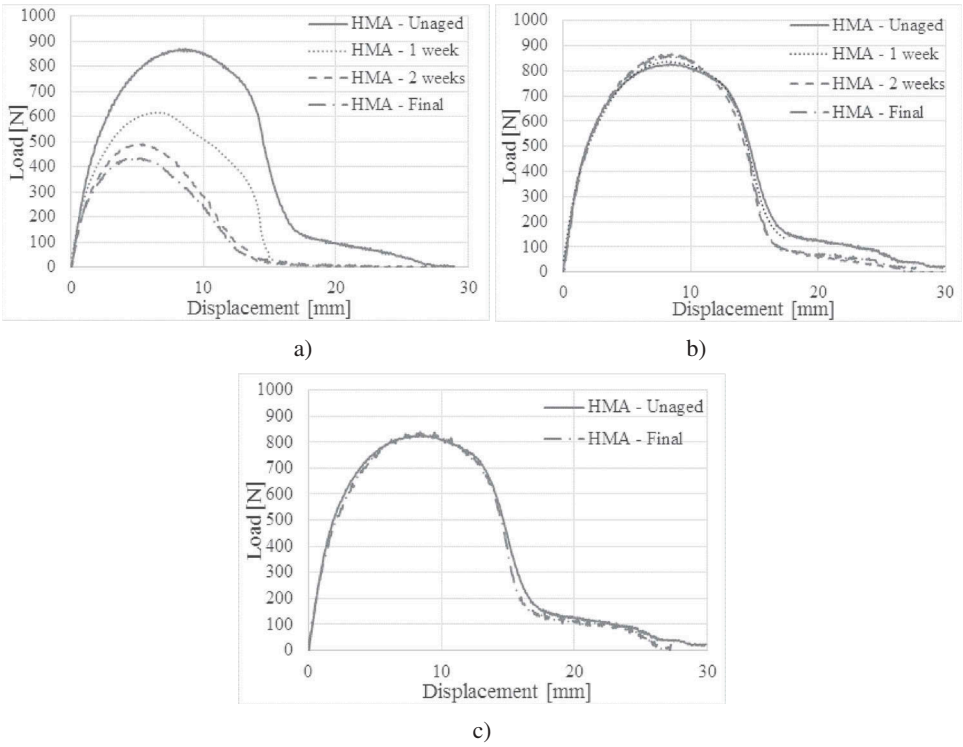

Figure 5. Mechanical behaviour of the pristine adhesive during the accelerated ageing cycles A (diagram a), B (diagram b) and C (diagram c).

Figure 5b reports the load-displacement curves during and at the end of the cycles B. As expected, the mechanical behaviour of the lap shear tests under ageing B shows a good response to humid conditions. This result was expected since the PP copolymer substrates bonded with polyolefin-based HMA form a hydrophobic system and thus this humid cycle connected to the relatively low temperature is not able to affect the mechanical properties of the adhesive joints.

These bonded joints showed a good response with the cycle C as well, see Figure 5c, in fact, representative curves of SLJ tests after the ageing cycle C are almost superimposed. This means that the exposure for a relatively low time at severe environmental conditions does not affect the mechanical properties of the adhesive joints. The values of the maximum loads after the cycle B shows that the load is slightly higher than the non-aged adhesive joints. Table 3 reports the maximum loads together with the standard deviations of the lap shear tests. The values of the standard deviations are higher for the values relative to the cycle A.

Figure 6 shows the fracture surfaces of the pristine adhesives after the ageing cycles A, B and C. Visual inspections of the fractured specimens display that the fracture surfaces of the pristine HMA do not change for the cycle B and C. The failure surfaces found in this study were similar to the ones obtained in.[7,8,23,27] On the other hand, the cycle A causes a decrease of the cohesive fracture zone. Furthermore, it can be noted that the colour of the adhesive changes during the cycle A. This could be due to the oxidation of the adhesive that as will be shown in the ATR-FTIR section. For this reason, the resistant section of the adhesive decreases and consequently the maximum sustained load. This behaviour is more evident in Figure 7, especially for the HMA_5% where it is clear that the only part that has a cohesive failure is limited to the nearly circular zone in the centre of the adhesive layer.

Table 3. Maximum loads (and standard deviations) of the pristine and the modified adhesives.

	Unaged	1 week	2 weeks	Final
		Pristine adhesive		
Cycle A	835 (22.52)	625 (73.00)	489 (79.23)	436 (70.31)
Cycle B	835 (22.52)	833 (39.85)	837 (31.30)	838 (21.70)
Cycle C	835 (22.52)	–	–	836 (33.79)
		HMA_3%		
Cycle A	872 (20.27)	649 (60.00)	459 (50.23)	436 (21.86)
Cycle B	872 (20.27)	871 (15.59)	871 (26.57)	875 (18.62)
Cycle C	872 (20.27)	–	–	868 (37.93)
		HMA_5%		
Cycle A	881 (30.85)	621 (52.74)	425 (15.01)	392 (30.00)
Cycle B	881 (30.85)	876 (22.31)	882 (16.46)	881 (20.41)
Cycle C	881 (30.85)	–	–	854 (43.68)
		HMA_10%		
Cycle A	895 (16.67)	597 (57.88)	448 (34.91)	432 (33.78)
Cycle B	895 (16.67)	845(22.26)	885 (12.29)	891 (20.41)
Cycle C	895 (16.67)	–	–	879 (16.65)

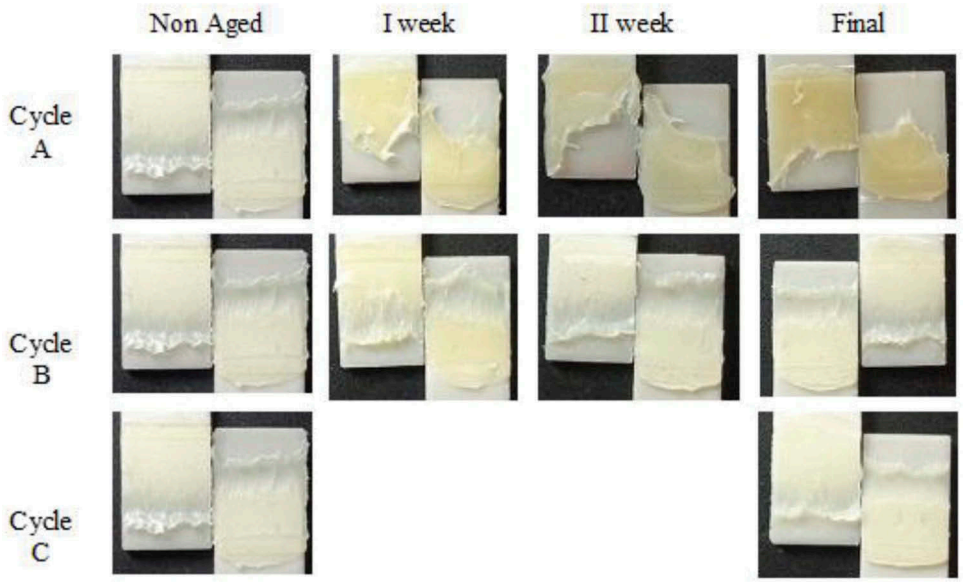

Figure 6. Fracture surfaces of the pristine HMA during and after the ageing cycles.

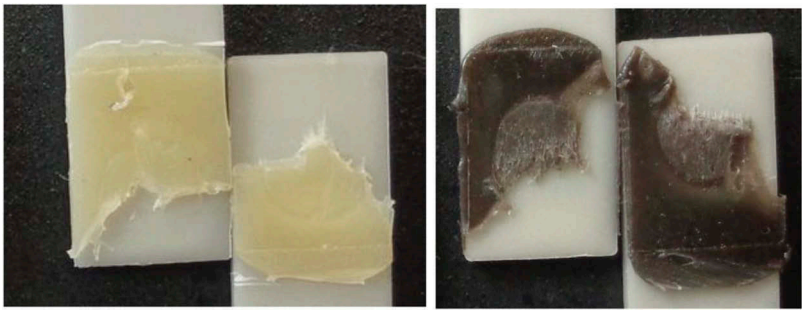

Figure 7. Fracture surfaces of HMA and HMA_5% at the end of the ageing cycle A.

Figure 8 shows the mechanical behaviour of the modified HMA_3% during the three different ageing cycles. The cycle A is again the most aggressive. In this case, the drop of the mechanical properties is slightly higher. The total drop of the maximum load for the ageing A after the 500 hours is 50%. The drops of the average maximum load at the end of each week period are respectively 25%, 21% and 2%. The decrease of the maximum load between the first and the second week is higher than for the pristine adhesive and the decrease between the second and the third one is slight. This is shown also by the curves relative to the 2 weeks and at the end of the cycle A are closer for this compound compared to the pristine adhesive. These two curves are almost superimposed. It seems that the presence of the nanoparticles quickens the ageing process. The ageing effect of HMA_3%, for the ageing B, is similar to the pristine adhesive. At the end

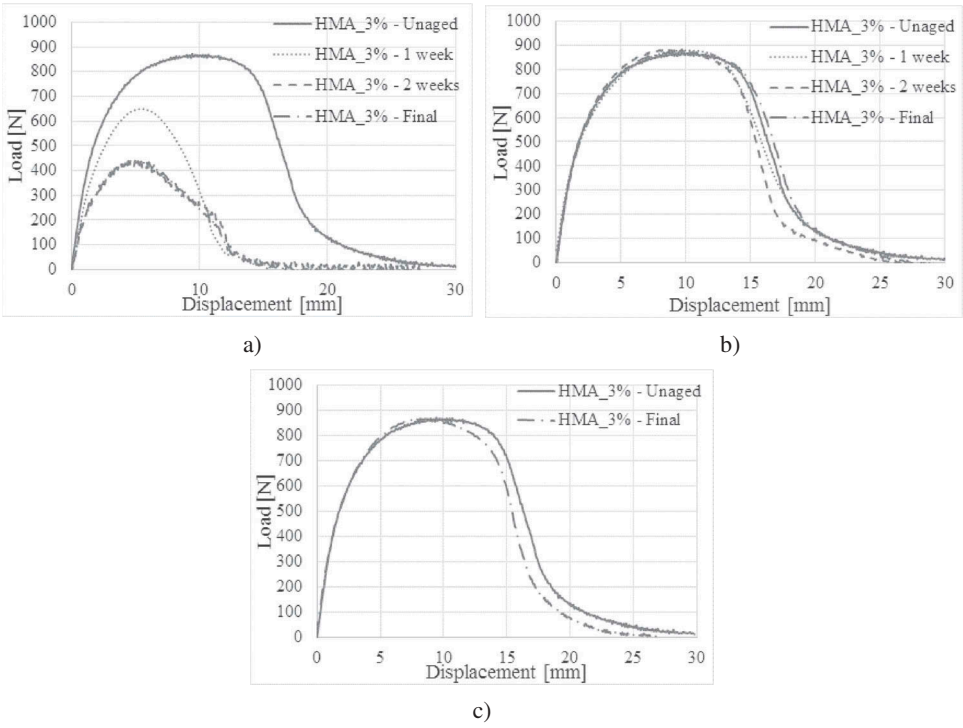

Figure 8. Mechanical behaviour of the HMA_3% wt. during the accelerated ageing cycles A (diagram a), B (diagram b) and C (diagram c).

of the ageing cycle, there is not a significant difference neither of the maximum values nor of the curve trends. The cycle C does not seem to lead to a change in the mechanical behaviour as for the pristine adhesive. However, the tail of the curve, on the right side, is slightly shorter compared to the non-aged specimens. This behaviour was not observed with the pristine adhesive. The values of the maximum loads and the relative standard deviation are reported in Table 3.

Figure 9 shows the fracture surfaces of HMA_3% after the ageing cycles. The visual inspections of the fracture surfaces show that the fracture mechanism does not change for the cycle B and C as for the pristine adhesive. On the other hand, the effect of the ageing cycle A for the HMA_3% is very similar to what has been observed with the pristine adhesive. In this case, since the colour of the modified adhesive is black, the reduction of the residual circle area, representative of the final resistance section, is more evident. Furthermore, it is noticeable the decrease of this section during the three weeks.

Figure 10 shows the mechanical behaviour of SLJs prepared with HMA_5% during and at the end of the three different ageing cycles. The cycle A is again the most aggressive. In this case, the final drop of the maximum load is the 55%, 5% higher than the previous ones. The reductions

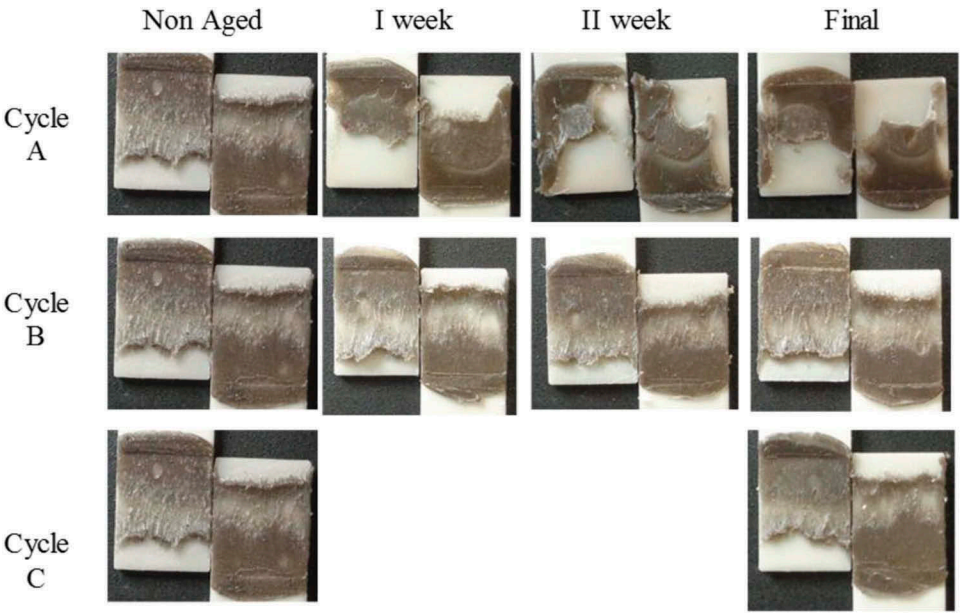

Figure 9. Fracture surfaces of HMA_3% during and at the end of the ageing cycles.

of the average maximum load at the end of each of the three weeks period are 29%, 22% and 3%, respectively. Thus, the mechanical behaviour of these adhesive joints is similar to the one prepared with HMA_3%. The maximum loads and the main trend of the curves remain almost constant during the ageing B. As for the HMA_3%, the tail on the right side, at the end of the cycle C, is slightly shorter. The trends for the cycle C reflect what has been observed for the joints prepared with the previous compounds, the maximum load is slightly lower. The values of the maximum loads and the relative standard deviation are reported in Table 3.

Figure 11 shows the fracture surfaces of HMA_5% after the ageing cycles. Visual inspection of fracture surfaces shows that they are very similar to the previous adhesive compounds. Again, the fracture surfaces of the specimens aged with the cycles B and C do not change. On the other hand, there is an increase of the adhesive separation for the specimens exposed to cycle A.

Figure 12 shows the mechanical behaviour of the joints bonded with HMA_10% at three different times during the three different ageing cycles. The cycle A is again the most aggressive. In this case, the final drop of the maximum load, for the ageing cycle A, is the 52%. The reductions of the average maximum load during the three weeks are 33%, 16% and 2%, respectively, that are reductions similar to the SLJs prepared with the previous nanomodified adhesives. After the second week and at the end of the cycle, the curves are significantly close. In the case of cycle B, the maximum loads are constant and the trends are superimposed. The trends of the cycle C reflect the trends of the

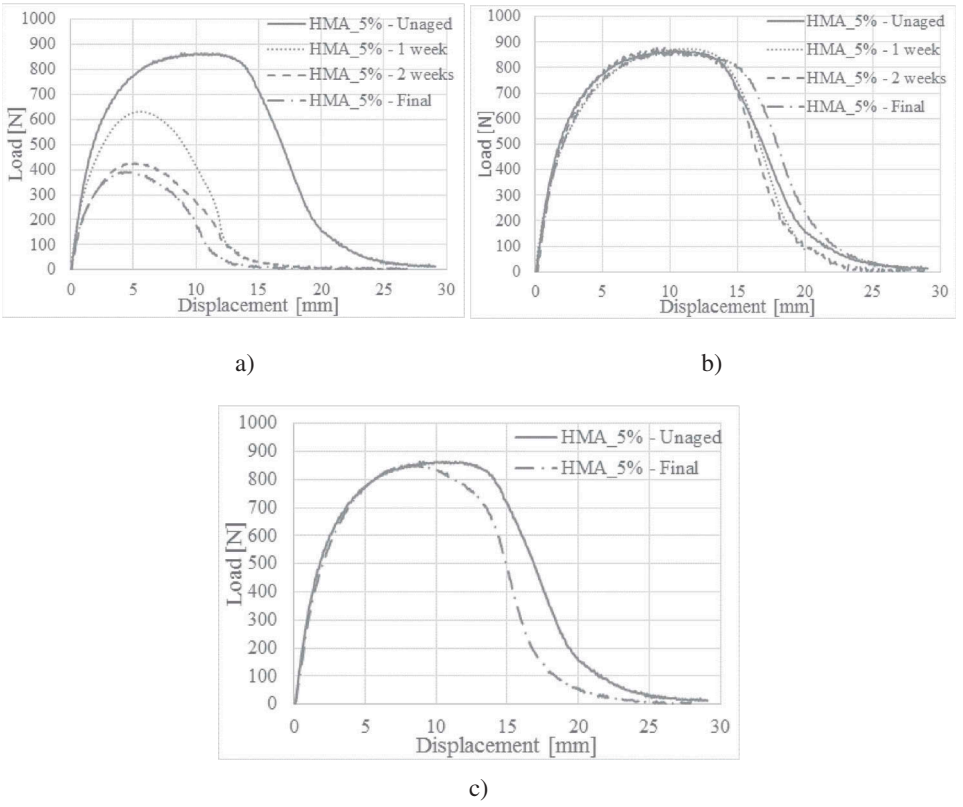

Figure 10. Mechanical behaviour of the HMA_5% during the accelerated ageing cycles A (diagram a), B (diagram b) and C (diagram c).

previous adhesive compounds where the maximum load is slightly lower at the end of the cycle and the right tail is shorter. The values of the maximum loads and the relative standard deviation are reported in Table 3.

The maximum values of the loads for all the adhesive compositions are in Table 3. This table illustrate the drop of the maximum strengths during the 500 h of the cycles A and B. The ageing cycle A leads to a final load decrease of 47%, 50%, 55% and 52% respectively for the pristine adhesive. Furthermore, the standard deviations relative to these cycle were higher for all the adhesive compositions.

Figure 13 shows the fracture surfaces of HMA_10% during and after the ageing cycles. Visual inspection of the fracture surface of HMA_10% during the ageing cycles are very similar to the previous ones. Again, the fracture surfaces of the specimens aged with the cycle B and C do not change. On the other hand, there is a decrease of the resistance area of the specimens exposed to cycle A.

Figure 14 reports the values of the normalised maximum loads for the four different adhesive compounds for the Cycle A as a function of the ageing

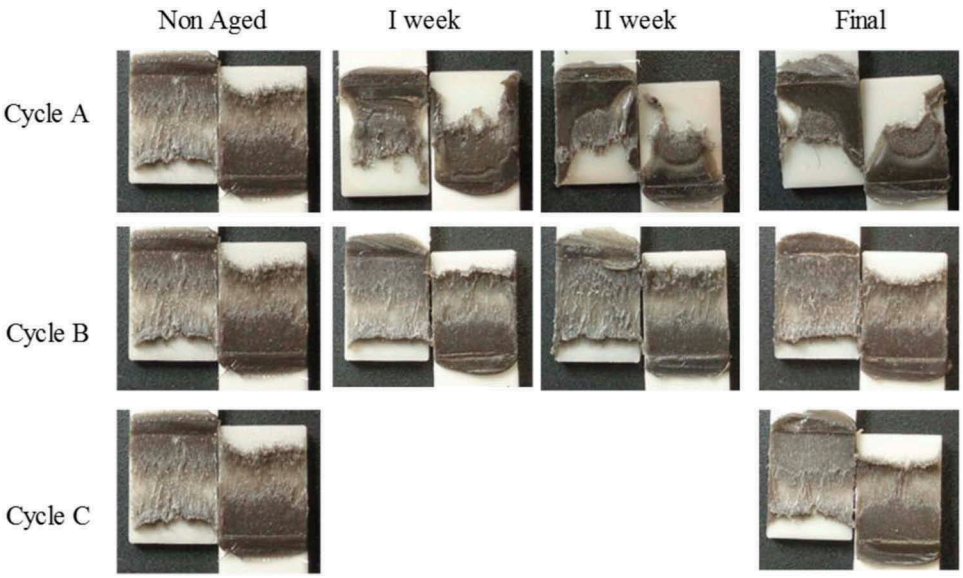

Figure 11. Fracture surfaces of HMA_5% during the ageing cycles.

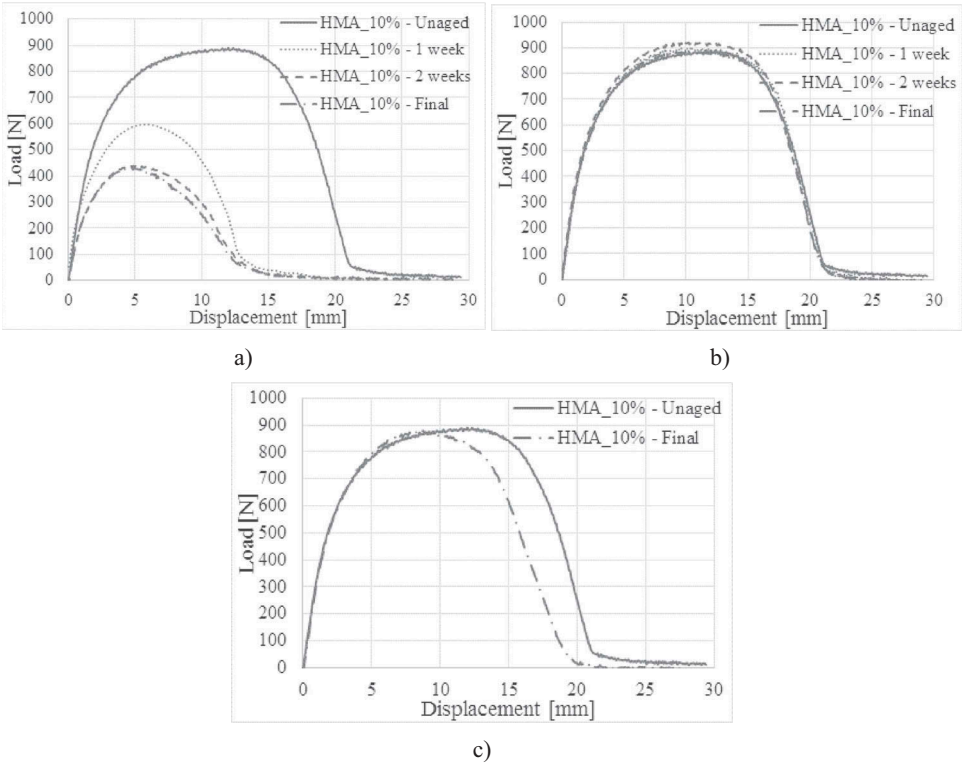

Figure 12. Mechanical behaviour of the HMA_10% during the accelerated ageing cycles A (diagram a), B (diagram b) and C (diagram c).

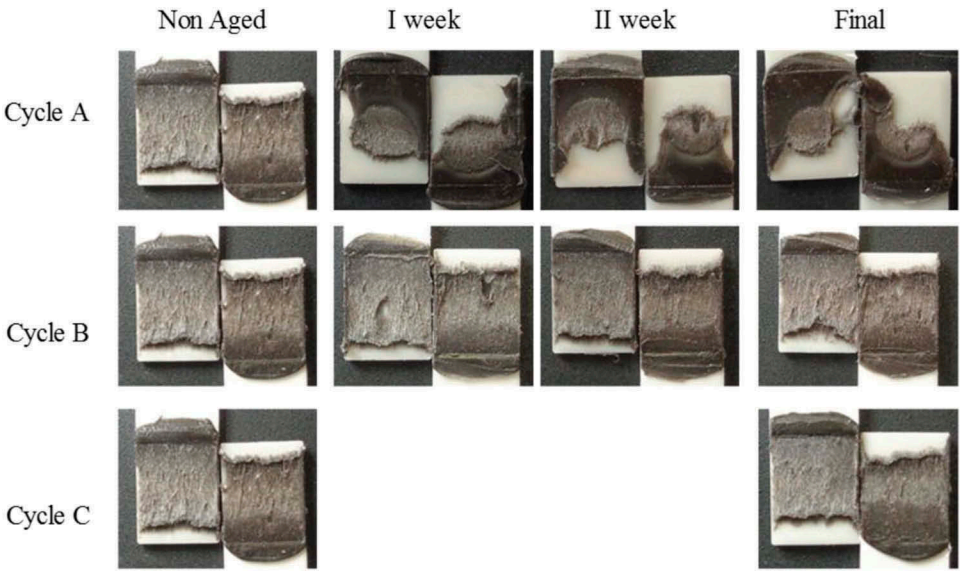

Figure 13. Fracture surfaces of HMA_10% during the ageing cycles.

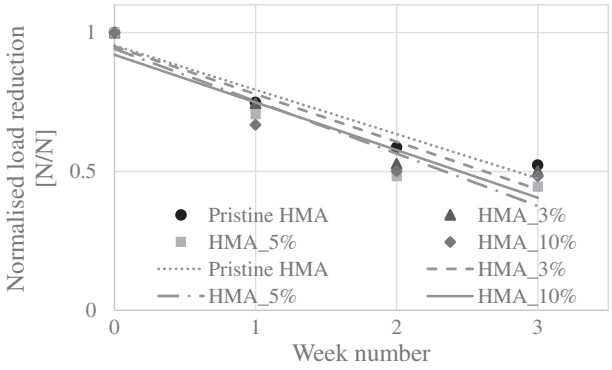

Figure 14. Linear regression of the normalised maximum loads for the ageing cycle A.

time over the 500 h together with their linear regressions. The values are normalised by the maximum load hence the first values are 1 for all the adhesive compounds then their progressive percentage decrease is visible. The trends of the linear regressions show that the reduction of the mechanical properties is quicker, although slightly quicker, for the nanomodified adhesives. The maximum loads of the nanomodified adhesives are very close between the second and third weeks as shown in the Table 3 as well.

3.4. *SEM analysis*

The SEM analysis has been carried out on non-aged specimens since the main aim of this analysis is to understand the dispersion of the particles into

the adhesive matrix. The ageing cycles are not so severe to change the particle dispersion. Figure 15 shows a representative SEM image at 500x magnification of HMA_10%. The largest white shining spots in Figure 15 are due to the presence of some deposed residuals attached to the adhesive surface before the SEM analysis. These residuals were analysed with the EDS associated with the SEM equipment and their compositions resulted to be $CaCO_3$ and SiO_2 that is typical of the dust.

In Figure 15, the tiny white spots are the iron oxide nanoparticles embedded in the HMA matrix, they were verified by EDS as Fe content. The distribution of these iron oxide fillers within the adhesive is almost uniform except for small areas that seem to be without particles. The total area without particles, evaluated through digital image processing, is equal to 854.1 μm^2 and it represents the 0.15% of the investigated area.

Figure 16a and 16b show SEM images of the modified adhesive at 5000x and at 10000x, respectively.

As can be seen in these images, nanoparticles tend to form small aggregates. The aggregate dimension was assessed at fifteen different locations in Figure 16a. In particular, the average particle size was found to be equal to 0.86 μm, with a standard deviation of 0.41 μm. The presence of these small aggregates is attributed to the nature of the particles that, before mixing, display a tendency to agglomerate as shown by Ciardiello et al..[27]

Figure 17 shows the particles dispersion of the HMA modified with 5% wt. of iron oxide. The presence of particle fillers is obviously lower compared to the 10% wt. The distribution seems to be uniform, the dimension of nanoparticles seems to be in accordance with the datasheet of the manufacturer. Unfortunately, this SEM did not permit to obtain bigger and clearer

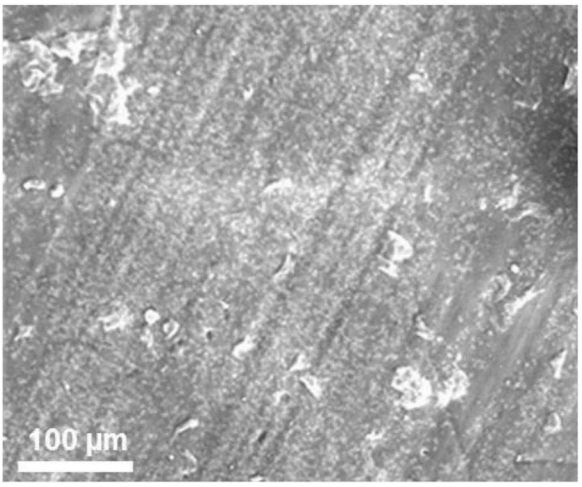

Figure 15. Representative SEM image at 500x of HMA_10%.

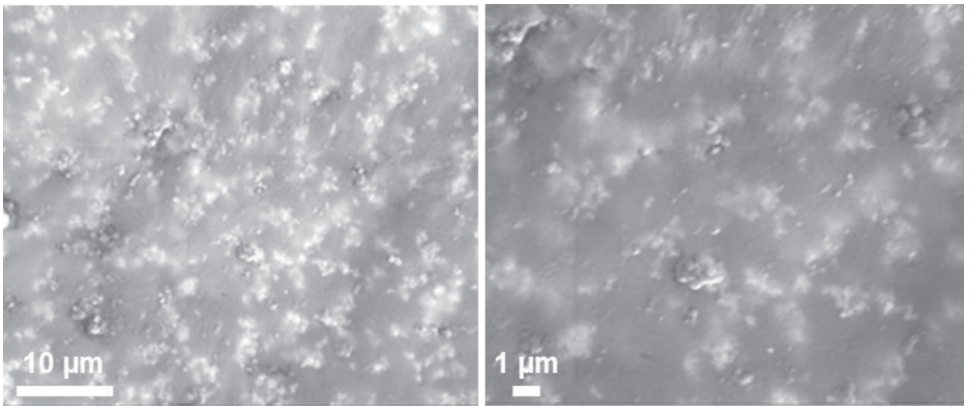

Figure 16. SEM images of HMA_10%: a) 5000x image; b) 10000x image.

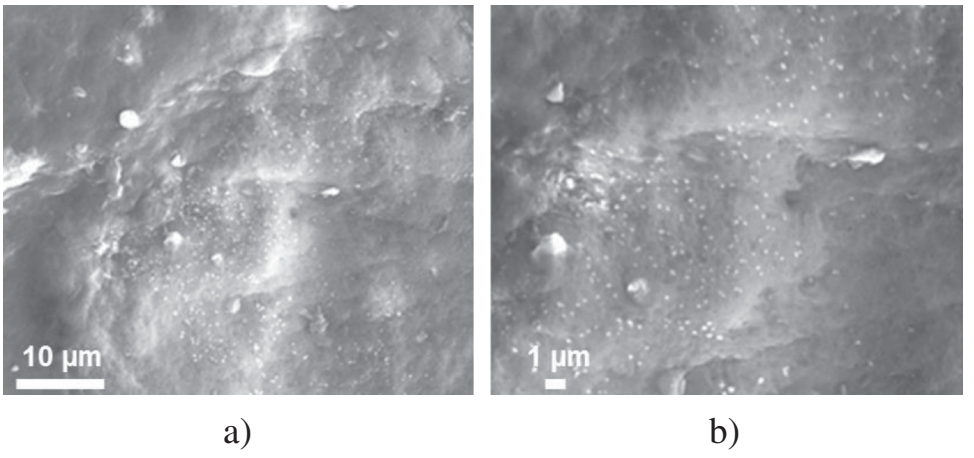

Figure 17. SEM images of HMA_5%: a) 5000x image; b) 10000x image.

magnification to assess the agglomerate sizes but the 10000x magnification shows a particles size that corresponds to what is visible in Figure 16.

Figure 18 illustrates the clearest SEM magnification of the HMA modified with 3% wt. at 10000x. As expected, the particles distribution results similar to the 5% wt.

3.5. *Effect of the ageing cycles on the separation time*

The effect of the ageing cycles on the electromagnetic induction process was studied as well. Figure 19 illustrates the comparisons of the separation times of the SLJs after the ageing cycles and the non-aged bonded joints. The debonding temperature for all the adhesive composition is 135°C. Results

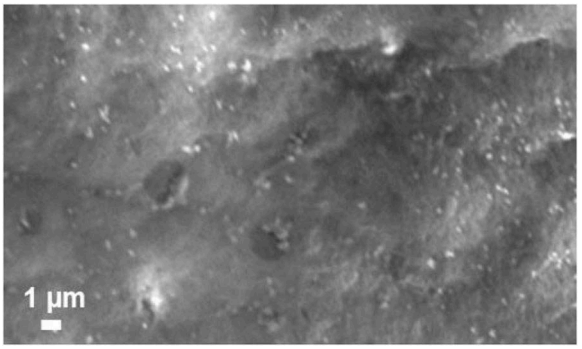

Figure 18. SEM images of HMA_3% at 10000x.

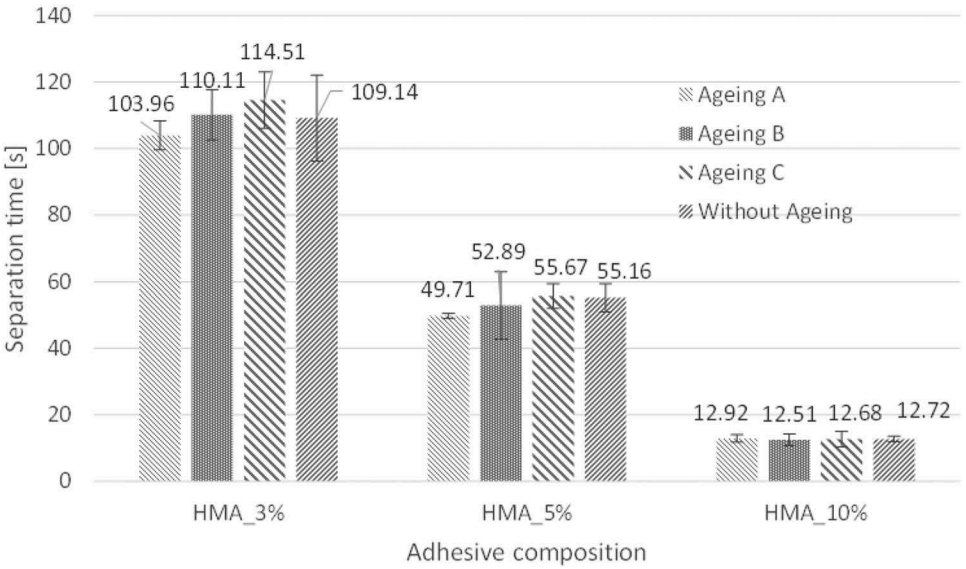

Figure 19. Effect of the ageing cycles on the separation time.

are shown for the three adhesive compositions: HMA_3%, HMA_5% and HMA_10%. As expected the values of the separation times decreases with the increase of the iron oxide content. It is worth of note that the separation times are characterised by a relatively small variation within the same percentage of iron oxide, so that one can conclude that the ageing process practically does not affect this type of performance. However, the lowest values for the HMA_3% and HMA_5% result for the specimens submitted to the ageing cycle A. The other values, for these two adhesive compositions, are very close to the non-aged values and within the scatter ranges. On the other hand, the values of the separation time relative to the HMA_10% have not a significant difference, the highest and the lowest values are into a 0.4 s scatter. Furthermore, these scatters are small if compared to the other two

adhesive compositions. Of course, the presence of the particles in the adhesive matrix is lower for HMA_3% and HMA_5% and, since the distribution is random, in the case of the HMA_10% the particles can be distributed in a way that allows a more efficient adhesive heating.

Figure 20 displays the surfaces separated by the induction heating process for the three adhesive compositions and the three ageing cycles. The separation surfaces of the unaged adhesive joints are compared with the ones separated after the ageing cycles. The most interesting aspect of Figure 20 is that the separation surfaces of cycles B and C are similar to the separation surfaces of the unaged joint, they exhibit a totally cohesive separation surface. On the other hand, the joints separated after the cycle A presented a mixed separation surface, that is adhesive and cohesive. These fracture surfaces present a circular cohesive zone that can be easily recognised and an area where the separation is adhesive, as highlighted for the fracture surfaces obtained from the SLJ tests that are relative to the same ageing cycle. These pictures show that the separation surface is cohesive in the inner part of the adhesive layer, while it is adhesive on the external part. This could be due to a detachment of adhesive due to the relatively high temperature of the ageing cycle A.

Interestingly, although the cohesive surface, that represents the residual resistance surface, is reduced a lot, there is not a huge decrease of the separation time, as depicted in Figure 19. This is because the separation occurs only when the adhesive is completely melted since the weight that has been used to initiate the slip is relatively low. HMA_5% and HMA_10% present some darker areas that are the areas where the adhesive melts earlier and where the separation starts.

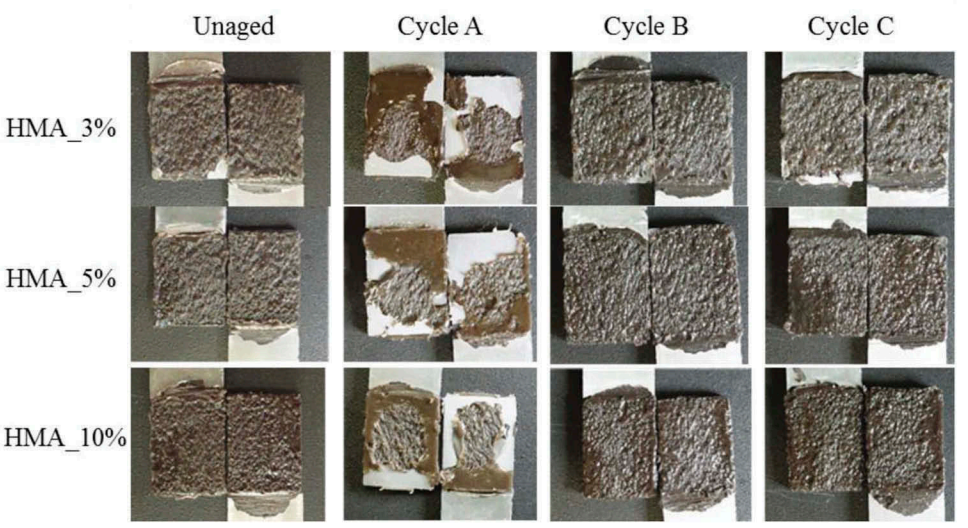

Figure 20. Separated surfaces of the disassembled joints.

3.6. *ATR-FTIR analysis*

Figure 21 shows ATR-FTIR (Attenuated total reflectance- Fourier-transform infrared spectroscopy) spectra of the pristine adhesive without ageing and at the end of the ageing cycles. The main aim of the ATR-FTIR spectra is to understand whether oxidation occurs in the specimen. The areas of major interest are in the wavelength range between 1800–1500 cm^{-1} and 1300–1100 cm^{-1}. In the first range it is possible to find the peaks due to C = O bond of ketones, carboxylic acids, esters, common oxidation products of polyolefines.[24] The magnification detail in the Figure illustrates that the oxidation peaks (at 1710 cm^{-1}, 1740 cm^{-1} and 1780 cm^{-1}) is higher for the ageing cycle A whereas is almost the same for the not aged sample and the others two cycles. In the range 1300–1100 $cm^{-1,}$ the peaks are relative to C-O bond[5], again connected to oxidation products. Again, the peaks are higher for the cycle A whereas the HMA specimens without ageing and with the others two ageing cycles have a similar absorbance.

Figure 22 shows the differences in the spectral absorbance of the modified HMA without ageing and with all the considered ageing cycles. The test conducted on the modified adhesives showed that this analysis is not adequate to detect oxidation of the modified adhesive because of the dark colour of the adhesive layer. In fact, Figure 22 shows that there is not a significant change of the curves, especially in the range 1000–2000 where the oxidation is visible, while mechanical tests showed that the oxidation affects modified adhesive as well.

4. Conclusions

Iron oxide particles have been added to a HMA adhesive in order to make possible separation of the joints by means of pulsating electromagnetic field. The paper reports the main results of a mechanical characterization

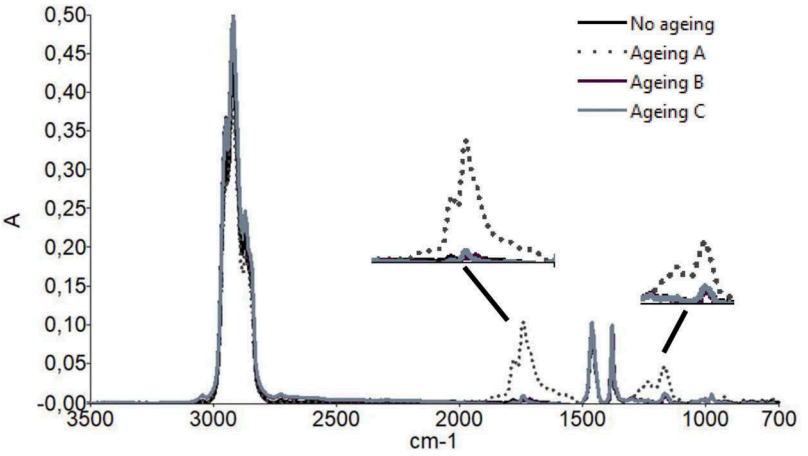

Figure 21. ATR-FT-IR spectra of the pristine HMA.

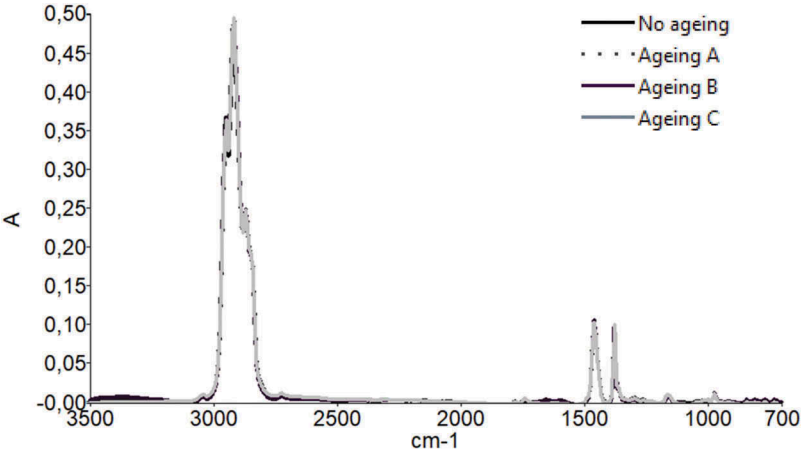

Figure 22. ATR-FT-IR spectra of the pristine HMA_10%.

campaign devoted to evaluate the influence of the nano-particle addition on the mechanical properties of the adhesive joints, with a particular attention on the effect of ageing cycles. Substrates are made of polypropylene, typically used in automotive applications.

Mechanical tests showed that the addition of the iron oxide (three different weight percentages, namely 3, 5 and 10%, have been considered) increases the maximum shear strength of the adhesive. The SLJ tests showed that the nanomodified adhesives display a more ductile behaviour, as well. This could be due to a toughening effect of the bondline and to an observed increase of the cohesive zone that brings to higher ultimate loads. The ultimate shear strength increases with the increase of the particles concentration.

The considered three different ageing cycles, namely cycle A,B and C, conducted on the adhesive joints showed that the nanomodified adhesives have differentiated behaviour with respect to the pristine HMA. In all the cases, the cycle A (500 hours at 90°C), that resulted to be the more severe, leads to a reduction of the maximum strength of around 50%. On the other hand, cycle B (500 hours at 40°C with 98% of relative humidity) and cycle C (24 hours at 80°C without RH, 24 hours at 40°C with 98% of RH and 24 hours at −40°C) did not change the mechanical properties with respect to the pristine HMA or, in some cases, lead to a slightly increase of the maximum load. This is probably mainly due to the considered HMA whose chemical composition include polyethylene that is melting at a temperature close to 90°C.

The performed FT-IR tests showed that this analysis procedure is very good in order to observe the oxidation level of the base adhesive, especially during the ageing A, but it is not able to recognise the change for the modified adhesive because of its black colour.

Finally the performed electromagnetic separation tests showed that the separation time is deeply affected by the amount of the nanoparticles

addition, with a relevant decrement of the separation time with the increment of the nanoparticle percentage, but is not significantly affected by the ageing cycle, even for the accelerated cycle A, that was the most aggressive cycles. This is probably due to the low value of the applied load that is able to separate the substrate only when the adhesive is completely melted.

References

[1] Adams, R. D.;. *Adhesive Bonding: Science, Technology and Applications*, Sawston: Woodhead Publishing, 2005.

[2] Belingardi, G.; Chiandussi, G. Stress Flow in Thin-Walled Box Beams Obtained by Adhesive Bonding Joining Technology. *Int. J. Adhes. Adhes*. 2004, *24*(5), 423–439. DOI: 10.1016/j.ijadhadh.2003.11.009.

[3] Belingardi, G.; Goglio, L.; Tarditi, A. On the Optimization of Single Lap Metal/Plastics Adhesive Joints. *Key Eng. Mater*. 2002, *221–222*, 161–172.

[4] Moritomi, S.; Watanabe, T.; Kanzaki, S. Polypropylene Compounds for Automotive Applications. *SUMITOMO KAGAKU" R&D Rep*. 2010, *1*, 1–16.

[5] Belingardi, G.; Brunella, V.; Martorana, B.; Ciardiello, R. Thermoplastic Adhesive for Automotive Applications. In *Adhesive – Application and Properties*, 1st ed.; Rudawska, A., Ed.; Intech: Rijeka, 2016; Vol. 1, pp 341–362.

[6] Lu, Y.; Broughton, J.; Winfield, P. A Review of Innovations in Disbonding Techniques for Repair and Recycling of Automotive Vehicles. *Int. J. Adhes. Adhes*. 2014, *50*, 119–127. DOI: 10.1016/j.ijadhadh.2014.01.021.

[7] Ciardiello, R.; Martorana, B.; Lambertini, V. G.; Brunella, V. Iron-Based Reversible Adhesives: Effect of Particles Size on Mechanical Properties. *Proc. Inst. Mech. Eng. Part C J. Mech. Eng. Sci*. 2018, *232*(8), 1446–1455. DOI: 10.1177/0954406217736552.

[8] Verna, E.; Cannavaro, I.; Brunella, V.; Koricho, E. G.; Belingardi, G.; Roncato, D.; Martorana, B.; Lambertini, V.; Alina Neamtu, V.; Ciobanu, R. Adhesive Joining Technologies Activated by Electro-Magnetic External Trims. *Int. J. Adhes. Adhes*. 2013, *46*, 21–25. DOI: 10.1016/j.ijadhadh.2013.05.008.

[9] Jeun, M.; Lee, S.; Kyeong Kang, J.; Tomitaka, A.; Wook Kang, K.; Il Kim, Y.; Takemura, Y.; Chung, K. W.; Kwak, J.; Bae, S. Physical Limits of Pure Superparamagnetic Fe_3O_4 Nanoparticles for a Local Hyperthermia Agent in Nanomedicine. *Appl. Phys. Lett*. 2012, *100*, 9. DOI: 10.1063/1.3689751.

[10] Ghazanfari, M. R.; Kashefi, M.; Shams, S. F.; Jaafari, M. R. Perspective of Fe_3O_4 Nanoparticles Role in Biomedical Applications. *Biochem. Res. Int*. 2016, *2016*, 1–32. DOI: 10.1155/2016/7108261.

[11] Néel, L.;. Theorie Du Trainage Magnetique Des Ferromagnetiques En Grains Fins Avec Applications Aux Terres Cuites. *Ann. Geophys*. 1949, *5*, 99–136.

[12] Moskowitz, B. M.; Frankel, R. B.; Walton, S. A.; Dickson, D. P. E.; Wong, K. K. W.; Douglas, T.; Mann, S. Determination of the Preexponential Frequency Factor for Superparamagnetic Maghemite Particles in Magnetoferritin. *J. Geophys. Res*. 1997, *102*(97), 22671. DOI: 10.1029/97JB01698.

[13] Kandasamy, G.; Maity, D. Recent Advances in Superparamagnetic Iron Oxide Nanoparticles (Spions) for in Vitro and in Vivo Cancer Nanotheranostics. *Int. J. Pharmaceutics*. 2015, 191–218. doi:10.1016/j.ijpharm.2015.10.058.

[14] Fiorillo, F.; Beatrice, C.; Coïsson, M.; Zhemchuzhna, L. Loss and Permeability Dependence on Temperature in Soft Ferrites. *In IEEE Trans. Magn.* 2009, *45*, 4242–4245. DOI: 10.1109/TMAG.2009.2025049.
[15] Banea, M. D.; Da Silva, L. F. M.; Carbas, R. J. C.; de Barros, S. Debonding on Command of Multi-Material Adhesive Joints. *J. Adhes.* 2017, *93*(10), 756–770. DOI: 10.1080/00218464.2016.1199963.
[16] Severijns, C.; de Freitas, S. T.; Poulis, J. A. Susceptor-Assisted Induction Curing Behaviour of a Two Component Epoxy Paste Adhesive for Aerospace Applications. *Int. J. Adhes. Adhes.* 2017, *75*, 155–164. DOI: 10.1016/j.ijadhadh.2017.03.005.
[17] Goglio, L.; Rezaei, M. Effect of Environmental Exposure on the Fracture Properties of an Epoxy Adhesive. *J. Adhes.* 2013, *89*(11), 807–821. DOI: 10.1080/00218464.2012.761569.
[18] Banea, M.; Da Silva, L. F. M.; Campilho, R. D. S. G.; Sato, C. Smart Adhesive Joints: An Overview of Recent Developments. *J. Adhes.* 2014, *90*(1), 16–40. DOI: 10.1080/00218464.2013.785916.
[19] Goglio, L.; Rezaei, M. Variations in Mechanical Properties of an Epoxy Adhesive on Exposure to Warm Moisture. *J. Adhes. Sci. Technol.* 2014, *28*(14–15), 1394–1404. DOI: 10.1080/01694243.2012.697392.
[20] Goglio, L.; Rezaei, M. Effect of Different Substrate Pre-Treatments on the Resistance of Aluminum Joints to Moist Environments. *J. Adhes.* 2013, *89*(10), 769–784. DOI: 10.1080/00218464.2012.759883.
[21] Pethrick, R.;. Design and Ageing of Adhesives for Structural Adhesive Bonding – A Review. *Proc. Inst. Mech. Eng. L.* 2015, *229*(5), 349–379.
[22] Viana, G.; Costa, M.; Banea, M. D.; Da Silva, L. F. M. A Review on the Temperature and Moisture Degradation of Adhesive Joints. *Proc. Inst. Mech. Eng. L.* 2017, *231*(5), 488–501.
[23] Koricho, E. G.; Verna, E.; Belingardi, G.; Martorana, B.; Brunella, V. Parametric Study of Hot-Melt Adhesive under Accelerated Ageing for Automotive Applications. *Int. J. Adhes. Adhes.* 2016, *68*, 169–181. DOI: 10.1016/j.ijadhadh.2016.03.006.
[24] Ciardiello, R.; Belingardi, G.; Martorana, B.; Fondacaro, D.; Brunella, V. A Study of Physical and Mechanical Properties of A Nanomodified Thermoplastic Adhesive in Normal and Accelerated Ageing Conditions. In ECCM 2016 – Proceeding of the 17th European Conference on Composite Materials, Munich, Germany; 2016.
[25] ISO 188:2011 Rubber, vulcanized or thermoplastic - Accelerated ageing and heat resistance tests.
[26] ASTM D5721 - Standard practice for air-oven aging of polyolefin geomembranes.
[27] Ciardiello, R.; Tridello, A.; Brunella, V. R.; Martorana, B.; Paolino, D. S.; Belingardi, G. Impact Response of Adhesive Reversible Joints Made of Thermoplastic Nanomodified Adhesive. *J. Adhes.* 2017. DOI: 10.1080/00218464.2017.1354763.
[28] Zhai, L.; Ling, G.; Li, J.; Wang, Y. The Effect of Nanoparticles on the Adhesion of Epoxy Adhesive. *Mater. Lett.* 2006, *60*(25–26), 3031–3033. DOI: 10.1016/j.matlet.2006.02.038.
[29] May, M.; Wang, H. M.; Akid, R. Effects of the Addition of Inorganic Nanoparticles on the Adhesive Strength of a Hybrid Solgel Epoxy System. *Int. J. Adhes. Adhes.* 2010, *30*(6), 505–512. DOI: 10.1016/j.ijadhadh.2010.05.002.